IONIC POLYMER-METAL COMPOSITES

THERMODYNAMICAL MODELLING AND FINITE ELEMENT SOLUTION

A Thesis

by

JAYAVEL ARUMUGAM

Submitted to the Office of Graduate Studies of
Texas A&M University
in partial fulfillment of the requirements for the degree of

MASTER OF SCIENCE

August 2012

Major Subject: Mechanical Engineering

IONIC POLYMER-METAL COMPOSITES

THERMODYNAMICAL MODELLING AND FINITE ELEMENT SOLUTION

A Thesis

by

JAYAVEL ARUMUGAM

Submitted to the Office of Graduate Studies of
Texas A&M University
in partial fulfillment of the requirements for the degree of

MASTER OF SCIENCE

Approved by:

Co-Chairs of Committee,	Arun Srinivasa
	J. N. Reddy
Committee Member,	Steven D. Taliaferro
Head of Department,	Jerald Caton

Major Subject: Mechanical Engineering

ABSTRACT

Ionic Polymer-Metal Composites

Thermodynamical Modelling and Finite Element Solution.

(August 2012)

Jayavel Arumugam, B.Tech., Indian Institute of Technology Madras

Co–Chairs of Advisory Committee: Dr. Arun Srinivasa
Dr. J. N. Reddy

This thesis deals with developing a thermodynamically consistent model to simulate the electromechanical response of ionic polymer-metal composites based on Euler-Bernoulli beam theory. Constitutive assumptions are made for the Helmholtz free energy and the rate of dissipation. The governing equations involving small deformations are formulated using the conservation laws, the power theorem, and the maximum rate of dissipation hypothesis. The model is extended to solve large deformation cantilever beams involving pure bending which could be used in the characterization of the material parameters. A linear finite element solution along with a staggered time stepping algorithm is provided to numerically solve the governing equations of the small deformations problem under generalized electromechanical loading and boundary conditions. The results are in qualitative and quantitative agreement with the experiments performed on both Nafion and Flemion based Ionic Polymer-Metal Composite strips.

TABLE OF CONTENTS

CHAPTER Page

LIST OF FIGURES

FIGURE Page

CHAPTER I

INTRODUCTION

A. Ionic Polymer Metal Composites

Materials exhibiting coupled phenomena such as temperature affecting mechanical deformation and vice versa (Shape Memory Alloys, thermo-elastic materials), could be put to intelligent use in many engineering applications. Such materials are classified as 'Smart'. Ionic Polymer Metal Composite (IPMC) strips [1] are an example of one such material. IPMC strips respond to electric potential applied across two electrodes (see Figure 1) and undergo mechanical deformation. Conversely, when the strip is bent, an electric potential is developed across the surface of the strip. Given its large bending deflection with low actuation voltage input property and the converse effect, IPMC strips show promise in engineering applications such as in actuators, sensors, and energy and force transducers [4]. Further IPMC strips have been used in space and planetary applications like soft robotic actuators (dust wipers [5]), biomedical applications (gastrointestinal endoscopic devices [6]), and artificial muscles [7]. A wider list of applications ranging from mechanisms, robotic toys and actuators, human machine interfaces, and planetary and medical devices can be found in the literature [8]. The practical difficulties involved and directions to address those difficulties are discussed in [5].

IPMC strips are made up of an ionic polymer, like Nafion (perfluorosulfonate made by DuPont) or Flemion (perfluorocarboxylate, made by Asahi Glass, Japan) [5], which has fixed anions in the polymer network. This inonomeric polymer network is neutralized with a ionic solution with solvents like water and cations like

---

The journal model is *IEEE Transactions on Automatic Control.*

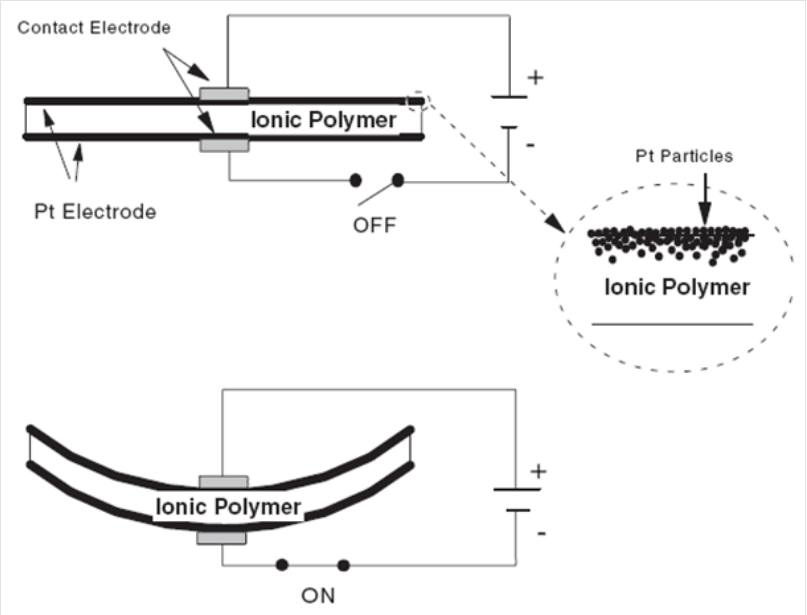

Fig. 1. A schematic of a typical IPMC strip and its actuation principle [1]. The IPMC is composed of an ionic polymer surface composited with a conductive medium like platinum for a few microns deep. The IPMC strip bends toward the anode when an electric potential is applied across the surface of the strip.

(Li^+) or tetrabutylaluminium ions (TBA^+). The surface is composited with a conductive medium like platinum or gold electrodes. A schematic of an IPMC strip is shown in Figure 1. When an electric potential is applied between the two surface electrodes, the IPMC strip bends. Redistribution of the mobile ions and water molecules due to various physical processes like diffusion, electrophoretic solvent transport and diffusion-deformation coupling gives rise to the electromechanical behavior.

The type of polymer base (Nafion or Flemion), the mobile cations [9], and the type of solvent [10] along with their composition affects the reponse of the IPMC strip. Under the application of a step voltage, Nafion based IPMC strips bend towards the anode. Flemion based IPMC strips show an initial fast bending movement towards the anode side and then a slow relaxation towards the cathode side. The tip displacement response, when a step voltage is applied differs, depending on the type of free mobile

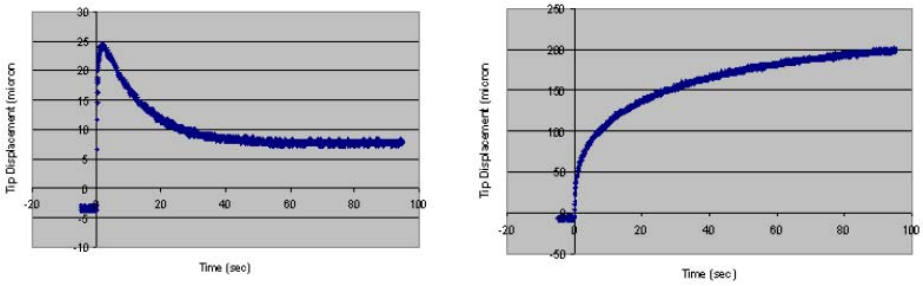

Fig. 2. Tip displacement measurement as a function of time for two Flemion based samples with different cations, Li^+ (left) and TBA^+ (right) [2].

cations even for a Flemion based sample, as shown in Figure 2.

B. Literature Review

A recent review of the current state of understanding of IPMC strips can be found in [11]. Experimental works include the study of the electromechanical responses of IPMC strips [9], their characterization, effect of different polymer base, solvent [10], and counterions on the chemical, physical, and electromechanical properties of IPMC strips and elucidation of underlying mechanisms. A review of different IPMC manufacturing techniques involving the compositing process and the surface electroding process can be found in [12].

Another area of research is development of theoretical models and concepts for the mechanisms that give rise to the coupled electro-mechanical response [13]. These models and theories are used to study how individual consituents of an IPMC strip affects the overall electromechanical response and various physiochemical and mechanical properties of IPMC strips. This facilitates the design of IPMC strips which show efficient, robust, and reliable response. Based on the micromechanical models like [14] it has been shown that it is possible to tailor the properties of IPMC strips [15]. Micromechanical models like [14] and multiscale models built on well established

principles [16] are one of the first reported studies to come up with hypotheses for actuation mechanisms.

Another approach in modelling is to macroscopically and phenomenologically capture the force-voltage-beam configuration response so that they can be used in the design and analysis of systems involving IPMC strips as components. Given that the state of many of these applications are still conceptual and under development, these models would be of significance.

C. Designer's Concern

The typical beam or plate like configuration of the IMPC is governed by the need for an electric field across the polymer. When the IPMC strips are used in actuators, information about the beam configuration as a function of time under the application of external mechanical loads and electric potential would be useful. This calls for an actuator model which relates electrical input to the mechanical output. When it is used in sensors, knowledge relating the electrical potential and charge developed across the surface of the strip as a function of time when the strip is deformed would be useful. This calls for a sensor model which relates mechanical input to the electrical output. State-space models offering ordinary differential equations to simulate these complex electromechanical responses are of immense value for material characterization and design of applications (as emphasized in [17] and [3]).

It would be beneficial in the design process to use a model based on physical principles which are thermodynamically consistent and addresses all the above requirements. Such a model, if versatile, would also be able to simulate different electromechanical responses (for eg. Figure 2).

D. Different Modeling Approaches

Amongst others, thermodynamically consistent ([18] and [19]), physics based ([20]), mixture theoretic [21] and micromechanical ([22]) models have been reported. Being interested more in the micromechanical behaviour rather than an input-output response, these models would be better suited for accurate analysis at final stages of design.

The need for a macroscopic beam model from a designer's perspective has been discussed in [17]. It provides one such model based on the micromechanical approaches ([14] and [23]). Such models, based on beam theories, are of particular interest due to usability and lesser computational costs. The drawback of the formulation given in [17] is that it is neither reduced to a state-space form nor shown to simulate the transient electromechanical response.

A phenomenological state-space actuator model relating the curvature of the beam to the charge accumulated at the surface is mentioned by [24]. A modification to that model which captures different electromechanical responses [3] has been proposed. Neither of the models reported in [17] and [24] ensures thermodynamic consistency as seen in [18] and [19].

E. Scope of the Present Study

Our hypothesis is that it is possible to develop a thermodynamically consistent model based on Euler-Bernoulli beam theory so that it simulates the electromechanical response of IPMC strips. We restrict ourselves to actuation in air.

Many models reported either capture the actuation behavior of IPMC strips or the sensing behavior ([25] and [26]). The model proposed here can be used for both actuation and sensing applications as in [27] and [17].

The approach proposed here finds trade-offs between simplicity and usability ([3] and [17]), usefulness of the state-space approach ([3]), ability to predict different responses ([28] and [3]), applicability in both sensing and actuation devices ([17]) while ensuring thermodynamical consistency ([18] and [19]) and making use of the study of underlying mechanisms ([16] and [14]). We also extend the model to handle large deformations involving pure bending since IPMC strips have very low modulus (of the order of GPa) and the deformations involved in actuator and sensor applications are high compared to beams designed using other smart materials like piezo-electric. This extension would better address this concern and would be useful for characterization of material paramaters from experimental data. We also provide an appropriate numerical technique to solve the small deformation beam problem under general loading conditions.

F. Contributions of the Thesis

Upon the completion of this work we will obtain,

- a thermodynamically consistent model to simulate the electromechanical reponse of IPMC strips based on classical beam theories using minimal constitutive variables.
- a model to handle large deformations involving pure bending.
- a linear Euler-Bernoulli finite element solution of the model proposed to handle general electromechanical loading and boundary conditions.

We analyze the performance of the model by comparing the simulation results with available experimental data reported ([3]). We show that a simple model could simulate the complex electromechanical behavior of IPMC strips.

G. Organization of the Thesis

- In Chapter II - Mechanisms, assumptions and small deformation bending problem formulation
- In Chapter III - Extension of the model to solve large deformation of cantilever beams
- In Chapter IV - Linear finite element solution
- In Chapter V - Results

CHAPTER II

MODEL FORMULATION

We define the kinematics for the deformation of the beam. We make constitutive assumptions for the Helmholtz free energy, the rate of dissipation. We derive the governing equations using the power theorem and the maximum rate of dissipation hypothesis subject to the constraint of mass conservation. We will start with a detailed list of mechanisms and simplifications that lead to the model formulation.

A. Mechanisms for Electro-mechanical Coupling

For the pruposes of this work, we will consider an IPMC strip to be a beam of length L and thickness $2h$ initially oriented along the x axis, and acted upon by external mechanical loads. An electric potential $V(x,t)$ is applied across the two plates. We are interested in obtaining the shape change in the beam due to the applied voltage and also the voltage obeserved due to the deformation of the beam by an external forces.

There are four parts to modelling the behaviour of IPMC strips namely,

- Mechanical behavior
- Electrical behavior
- Diffusion and electrophoresis
- Coupling between the above three

Under the actions of the external mechanical loads and the application of the electric potential across the electrode surface, redistribution of water molecules and

cations occur, which cause the strip to bend. This redistribution of particles have been reported (in [14] and [16]) to be due to the following processes,

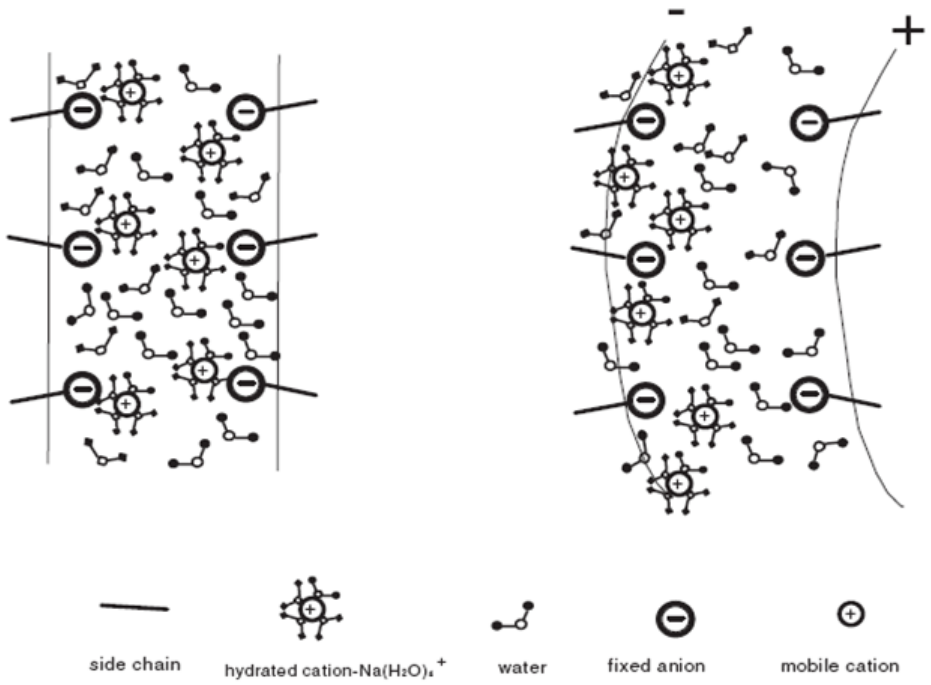

Fig. 3. Schematic of an ionic gel cantilever beam [1]. When an electric potential is applied between the two electrodes, an electric field is created within the strip. This electric field results in the movement of ions and the solvent molecules.

- diffusion of mobile cations and water molecules due to a gradient in chemical potential.
- electrophoresis - the motion of charged particles dispersed in a solvent under the influence of an electric field. The ions are hydrated and hence the movement of ions also result in the movement of water molecules [14].
- moment of water molecules and cations due to diffusion-deformation coupling.

These aspects are schematically shown in Figure 3.

B. Assumptions

We make the following assumptions in the formulation of the model.

- IPMC strips are thin and hence we neglect the effects of shear strain and formulate a Euler-Bernoulli beam theory.
- Water molecules move due to diffusion-deformation coupling and we neglect this effect for the mobile cations following [16].
- The electrical behaviour of IPMC strips in a circuit has been modelled using equivalent electrical circuits ([29], [30], [3]). We simplify this approach by considering just a resistor and a capacitor in series for the equivalent electrical circuit. We will show that this simplication, with respect to other effects considered in the model, is sufficient to simulate the electrical behaviour.
- The concentration field is assumed to vary linearly along a given cross section. This assumption has been already reported in [17].
- Diffusion of water molecules along the length of the beam is neglected and only that which occurs along any lateral section of the beam is considered. Similar assumptions have been made by [17] where they consider movement of cations only along the lateral section of the beam.
- Restricting the IPMC actuation and sensing in air, we consider no mass flux in and out of the strip.
- Kinetic energy/mass effect of the beam neglected as the inertial effects are too fast (of the order of micro seconds) compared to the time scale of the electromechanical response (order of seconds) that we are interested in.

C. Kinematics

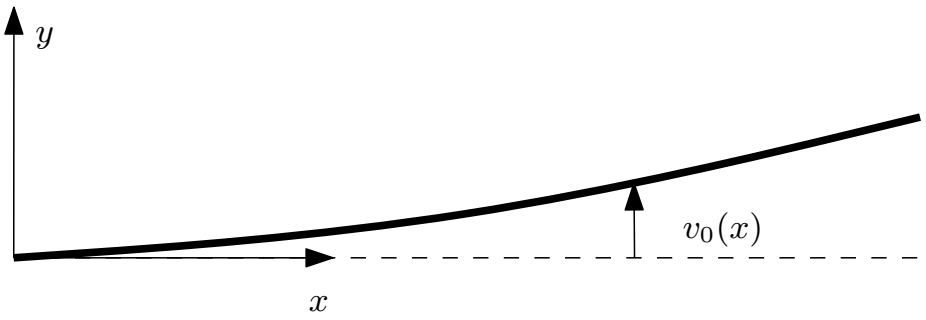

Fig. 4. Schematic of a beam showing the kinematics.

The x and y displacements of the centerline of the beam due to the combination of external load and the electric field is given by (shown in Figure 4)

$$u_1(x,y) = -yv_0'(x) \tag{2.1a}$$

$$u_2(x,y) = v_0(x) \tag{2.1b}$$

where $(.)'$ denotes derivative with respect to x. The linearized strains are given by

$$\epsilon_{xx} = -yv_0''(x), \quad \epsilon_{yy} = 0, \quad \epsilon_{xy} = 0 \tag{2.2}$$

Let $C(x,y,t)$ be the concentration of the water and it is assumed to be of the form

$$C(x,y,t) = C_0(x,t) + yC_1(x,t) \tag{2.3}$$

Next, we make constitutive assumptions for the Helmholtz free energy and the rate of dissipation. We make use of these kinematics to enforce conservation of mass and to derive the governing equations from the constitutive assumptions.

D. Helmholtz Free Energy

We consider a Helmholtz free energy formulation for the IPMC beam problem. The beam is assumed to be a combination of an electrical circuit and a poro-elastic beam. We model the response of IPMC strips in an electrical circuit as a combination of a capacitor and a resistor in series. Poro-eleastic beam refers to an elastic beam with a diffusing species where diffusion and deformation are coupled. We consider two types of coupling terms in the free energy.

- Coupling between the concentration of water molecules and the mechanical deformation as shown in [16].
- Coupling between the variation in water concentration and the charge at the surface. It is noted that the cations move under the influence of electric field which appears due to the charge developed at the surface electrodes. As stated earlier, water molecules also move as the cations move due to hydration.

Similar to [31], we assume a quadratic form for the Helmholtz free energy for the diffusion-deformation coupled problem. It invoves poro-elastic energy, an energy term for mixing of the diffusing species (water), electrostatic energy similar to the energy of a capacitor $q^2/2p$, and a coupling term $yDCq$. The Helmholtz free energy per unit volume of the IPMC beam is

$$\psi = \frac{E}{2}\left(\epsilon_{xx} - kC\right)^2 + \frac{E}{2}\left(\epsilon_{yy} - kC\right)^2 + \left(\frac{B - Ek^2}{2}\right)C^2 + \frac{q^2}{2p} + yDCq \tag{2.4}$$

where E is the Young's modulus of the beam, p is the capacitance of the beam, k is the coeficient of diffusion expansion, D is a coupling constant, and B is a constant relating concentration to the chemical potential.

The sresses, the chemical potential (which are similar to [31]) and the electric potential for the form of Helmholz free energy assumed above are given by

$$\sigma_{xx} = \frac{\partial \psi}{\partial \epsilon_{xx}} = E(\epsilon_{xx} - kC) \tag{2.5a}$$

$$\sigma_{yy} = \frac{\partial \psi}{\partial \epsilon_{yy}} = E(\epsilon_{yy} - kC) \tag{2.5b}$$

$$\mu = \frac{\partial \psi}{\partial C} = (B + Ek^2)C - Ek(\epsilon_{xx} + \epsilon_{yy}) + yDq \tag{2.5c}$$

$$V = \frac{\partial \psi}{\partial q} = \frac{q}{p} + yDC \tag{2.5d}$$

Integrating across a given cross-section of the beam while making use of the kinematic assumptions [(2.2) and (2.3)], we get the Helmholtz free energy per unit length of the beam as

$$\psi = \frac{EI}{2}\left(v_0''\right)^2 + EIkv_0''C_1 + \left(\frac{B + Ek^2}{2}\right)IC_1^2 + DIC_1q + \frac{q^2}{2p} + 2bh\left(\frac{B + Ek^2}{2}\right)C_0^2 \tag{2.6}$$

where I is the moment of inertia of the beam.

E. Enforcing Conservation of Mass for the Diffusing Species

Mass flux is solved using a finite volume approach. Two control volumes, one at the top half of the beam and the other at the bottom half, as shown in the Figure 5 was considered. This allows for the flux of the diffusing species between the top half and the bottom half of the beam.

Let the concentration values at the centre of top half and bottom half be C_t and C_b respectively. They are given by

$$C_t = C_0 + \frac{h}{2}C_1, \quad C_b = C_0 - \frac{h}{2}C_1 \tag{2.7}$$

Since the concentration is assumed to be linear, the rate of change of concentration

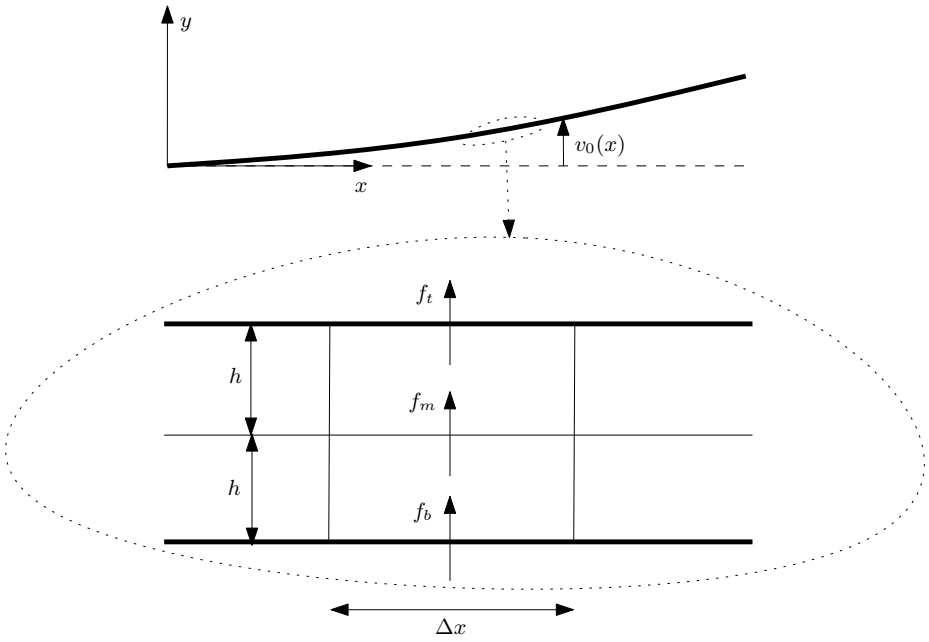

Fig. 5. Schematic showing the notation of flow variables and the two control volumes in a part of the beam.

in each volume is given by the rate of change of C_t and C_b times the volume. Then conservation of mass over each control element for the flux assumed is

$$hb\Delta x\dot{C}_t = -f_t\Delta x + f_m\Delta x, \quad hb\Delta x\dot{C}_b = f_b\Delta x - f_m\Delta x \tag{2.8}$$

Solving for $\dot{C}_1$ and $\dot{C}_2$ using (2.7),

$$\dot{C}_0 = \frac{1}{2h}(-f_t + f_b), \quad \dot{C}_1 = \frac{1}{h^2}(-f_t - f_b + 2f_m) \tag{2.9}$$

Assuming that $f_t = f_b = 0$ we obtain

$$\dot{C}_0 = 0 \tag{2.10}$$

$$\dot{C}_1 = \frac{2}{h^2}f_m \tag{2.11}$$

Since there is mass flux in and out of the IPMC strip when it is immersed in water, this assumption restricts the use of the model to actuation and sensing in air. It

is noted that by assuming $f_t = f_b = 0$, the beam becomes a closed system with respect to mass flux justifying the Helmholtz potential formulation rather than a Gibbs potential formulation.

F. Rate of Dissipation

Three forms of dissipation are considered namely,

- dissipation due to flow of charge (resistive heating).
- dissipation due to flow of water molecules (diffusion). Dissipation similar to this form has been reported [32].
- dissipation due to convective heating. Due to this term, the flow of charge and the flow of water molecules are coupled. This coupled term models the effect of movement of water molecules due to flow of current (movement of hydrated cations as discussed earlier).

The rate of dissipation 'ξ' is given by

$$\xi = Q_1 f_m^2 + R\dot{q}^2 + 2S_1 f_m \dot{q} \tag{2.12}$$

where R is the resistance, Q_1 and S_1 are constants.
Explicitly using the mass conservation constraint on C_1 in equation (2.11)

$$\xi = Q\dot{C}_1^2 + R\dot{q}^2 + 2S\dot{C}_1\dot{q} \tag{2.13}$$

where Q is constant. This form for the rate of dissipation is positive when $Q \geq 0$ & $R \geq 0$ & $QR \geq S^2$, the condition which ensures thermodynamic consistency.

G. Governing Equations

Using the maximum rate of dissipation hypothesis [33], the mechanical equilibrium equations and the transient response of q and C_1 are obtained (as shown in appendix A).

Mechanical equilibrium equation for the beam is given by

$$EI(v_0'''' + kC_1'') = w \tag{2.14}$$

along with the natural and essential boundary conditions

$$\begin{aligned} &(EI(v_0'' + kC_1) - M)\,\dot{v}_0'|_{x=0} = 0, \quad (EI(v_0'' + kC_1) - M)\,\dot{v}_0'|_{x=L} = 0 \\ &(EI(v_0''' + kC_1') - F)\,\dot{v}_0|_{x=0} = 0, \quad (EI(v_0''' + kC_1') - F)\,\dot{v}_0|_{x=L} = 0 \end{aligned} \tag{2.15}$$

At a given cross section of the beam

$$R\dot{q} + S\dot{C}_1 = V - \frac{q}{p} - DIC_1 \tag{2.16}$$

$$Q\dot{C}_1 + S\dot{q} = -EIkv_0'' - (BI + EIk^2)C_1 - DIq \tag{2.17}$$

$$\dot{C}_0 = 0 \tag{2.18}$$

Solving (2.14) using the boundary conditions in (2.15) and assuming the concentration profile doesn't vary across the length of the beam, we get the pure bending solution for the small deformation problem to be

$$v_0(x,t) = \frac{1}{2}\left(\frac{M}{EI} - kC_1(t)\right)x^2 \tag{2.19}$$

In the next chapter, we build on this small deformation model to formulate large deformation problems in cantilever beams. In chapter IV, we propose a linear finite element solution and a time stepping scheme to numerically solve equations (2.14), (2.16) and (2.17)

CHAPTER III

LARGE DEFORMATION

Cantilever beams are mostly used in the characterization of the electromechanical response of IPMC strips. We define the kinematics using an alternate coordinate system for the beam which allows us to solve large deformation problems in cantilever beams easily. We appropriately modify the constitutive assumptions made in the previous chapter using the new kinematic variables and derive the governing equations. We propose a numerical method based on finite difference to solve the governing equations. We also introduce a staggered time stepping scheme to solve the coupled transient problem.

A. Helmholtz Energy and Rate of Dissipation

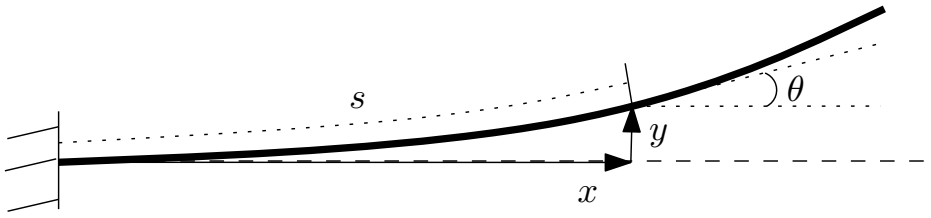

Fig. 6. Schematic of a beam showing the kinematic variables in the large deformation pure bending formulation.

We use an arc-length formulation for the beam problem with s being the arc-length, $\theta(s)$ being the angle made by the beam with the underformed configuration and $\kappa(s)$ the curvature of the beam. A schematic of such a beam is shown in Figure 6. Let us consoder a beam initially lyring across the x axis acted upon by an applied electric potential $V(s)$ and an end moment M.

The x and y coordinates are related to the θ and s by

$$\frac{dx}{ds} = cos(\theta), \quad \frac{dy}{ds} = sin(\theta) \tag{3.1}$$

Similar to (2.6) the Helmholtz free energy is assumed to be

$$\begin{aligned}\psi =& \frac{EI}{2}\left(\frac{d\theta(s)}{ds}\right)^2 + EIk\frac{d\theta(s)}{ds}C_1(s) + \left(\frac{B+Ek^2}{2}\right)IC_1(s)^2 + DIC_1(s)q(s) \\ &+ \frac{q(s)^2}{2p} + 2bh\left(\frac{B+Ek^2}{2}\right)C_0(s)^2\end{aligned} \tag{3.2}$$

where I is the moment of inertia of the beam.

The dissipation is assumed similar to (2.13) with C_1 and q begin functions of s

$$\xi = Q\dot{C}_1(s)^2 + R\dot{q}(s)^2 + 2S\dot{C}_1(s)\dot{q}(s) \tag{3.3}$$

B. Governing Equations

Using the maximum rate of dissipation hypothesis [33], the mechanical equilibrium equations and the transient response of $q(s)$ and $C_1(s)$ are obtained (as shown in the appendix B).

Mechanical equilibrium equation for the beam is given by,

$$\frac{d^2\theta(s)}{ds^2} + k\frac{dC_1(s)}{ds} = 0 \tag{3.4}$$

along with the natural and essential boundary condistions

$$\left(EI\frac{d\theta(s)}{ds} + EIkC_1(s) - M\right)\dot{\theta}\Big|_{s=0} = 0, \quad \left(EI\frac{d\theta(s)}{ds} + EIkC_1(s) - M\right)\dot{\theta}\Big|_{s=L} = 0 \tag{3.5}$$

At a given cross section of the beam

$$R\dot{q}(s) + S\dot{C}_1(s) = V(s) - \frac{q(s)}{p} - DIC_1(s) \tag{3.6}$$

$$Q\dot{C}_1(s) + S\dot{q}(s) = -EIk\frac{d\theta(s)}{ds} - (BI + EIk^2)C_1(s) - DIq(s) \tag{3.7}$$

$$\dot{C}_0(s) = 0 \tag{3.8}$$

When $V(s)$ is the same throughout the beam, solving (3.4), C_1 is assumed to be constant throughout the length of the beam, we get

$$\theta(s,t) = \left(\frac{M}{EI} - kC_1(t)\right) s \tag{3.9}$$

C. Numerical Scheme

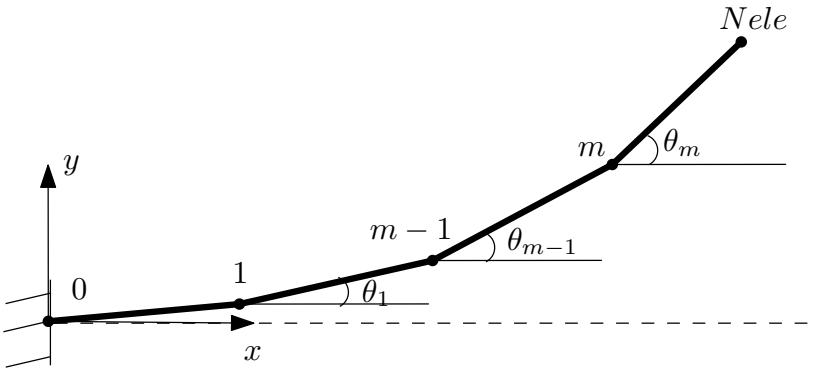

Fig. 7. Cantilever beam showing the spatial discretization.

To handle different but constant curvatures at different parts of the beam, such as when V(s) a constant but different at different parts of the beam as in $V(s) = 1\ for\ s = 0\ to\ L/2,\ V(s) = -1\ for\ s = L/2\ to\ L$, we use a finite difference scheme. The beam is discretized into $Nele$ nodes and each node is a discrete angle θ_i as shown in Figure 7. *We use superscripts and subscripts to denote time and spatial discretization respectively.* The spacial derivaties are approximated using the

following finite difference scheme, where m denote the spatial discretization.

$$\frac{d\theta}{ds} = (\theta_m - \theta_{m-1})/\Delta s \tag{3.10}$$

The x and y coordinates are apporimated using

$$x_m = x_{m-1} + cos(\theta_m)\Delta s, \quad y_m = y_{m-1} + sin(\theta_m)\Delta s \tag{3.11}$$

The time derivaties are approximated using the following finite difference scheme, where n denote the time discretization.

$$\dot{C}^n_{1,m} = (C^n_{1,m} - C^{n-1}_{1,m})/\Delta t, \quad \dot{q}^n_m = (q^n_m - q^{n-1}_m)/\Delta t \tag{3.12}$$

It is noted that the concentration and charge change at each element are independent of that in other elements. Hence this set of ODEs can be solved in parallel.

D. Transient Problem

Two types of time stepping schemes have been used in the literature to numerically solve coupled problems, such as diffusion-deformation. They are

- *Monolithic schemes* - the diffusion and deformation problem is solved together
- *Staggared scheme based on operator-split technique* - the diffusion and deformation problem are solved in two seperate steps. In one step which is purely elastic, the deformation is updated holding the concentration and charge fixed. In the other step which is purely dissipative, the concentration and charge are updated keeping the deformation fixed.

We use a staggered time stepping algorithm. The details of the algorithm are shown in Algorithm 1

Algorithm 1 Implementation of the Iterative Time-Stepping Scheme

1: Input: displacements at each node θ_i^0 where $i = 0, 1, 2, ..., Nele$, concentration slopes at each element $C_{1,j}^0$, charge at each element q_j^0 where $j = 1, 2, ..., Nele$, time step of integration Δt, Model parameters, Tolerance TOL.

2: Initialization

Set $\theta_i^n = \theta_i^0$, $C_{1,j}^n = C_{1,j}^0$, $q_j^n = q_j^0$

3: **while** $norm(\Delta\theta) <= TOL$ **do**

4: Find $C_{1,j}^{n+1}$ and q_j^{n+1} using θ_i^n, $C_{1,j}^n$ and q_j^n

5: Find θ_i^{n+1} using θ_{i-1}^{n+1}, $C_{1,j}^{n+1}$ and q_j^{n+1}

6: Set $\theta_i^n = \theta_i^{n+1}$, $C_{1,j}^n = C_{1,j}^0$, $q_j^n = q_j^0$, $\Delta\theta = \Sigma(\theta_i^{n+1} - \theta_i^n)$

7: **end while**

The formulation proposed here could handle only cantilever beams with certain loading conditions. In the next chapter, we formulate a numerical scheme to solve the small deformation model proposed in chapter II under general electromechanical loading and boundary conditions.

CHAPTER IV

LINEAR FINITE ELEMENT SOLUTION

We develop a linear Euler-Bernoulli finite element beam model for the electromechanical response of IPMC strips which could handle general mechanical and electrical loading conditions. First we develop a linear finite element solution, then discuss the staggered time stepping algorithm used to solve the coupled transient response.

A. Discretization

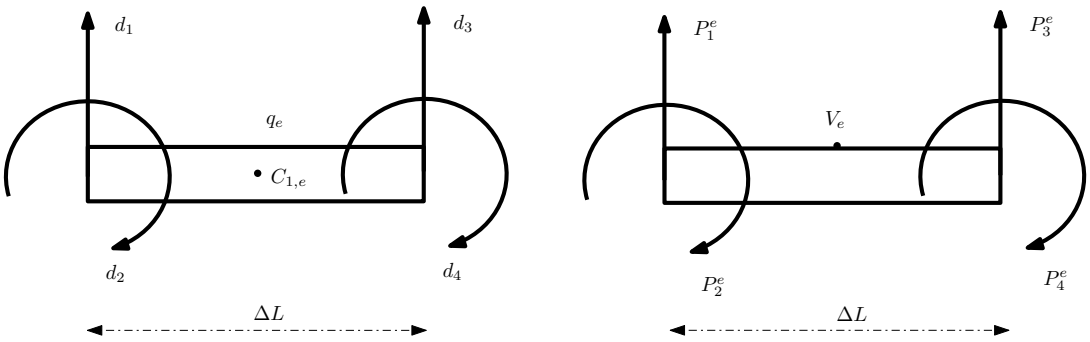

Fig. 8. The modified Euler-Bernoulli beam element showing the generalized displacements and forces.

The IPMC beam is discretised using conventional generalized displacements d_i and forces P_i. The displacements are interpolated using *Hermite cubic interpolation* functions N_i. In addition to the conventional discretization for the beam, each element is assigned a discretized average concentration C_e, charge q_e and electric potential V_e as shown in Figure 8

$$u = N_i(x)d_i \tag{4.1}$$

The *Hermite cubic interpolation* functions N_i are given by

$$N_1 = \frac{1}{\Delta L^3}(2x^3 - 3x^2\Delta L + \Delta L^3) \tag{4.2a}$$

$$N_2 = \frac{1}{\Delta L^3}(x^3\Delta L - 2x^2\Delta L^2 + x\Delta L^3) \tag{4.2b}$$

$$N_3 = \frac{1}{\Delta L^3}(-2x^3 + 3x^2\Delta L) \tag{4.2c}$$

$$N_4 = \frac{1}{\Delta L^3}(x^3\Delta L - x^2\Delta L^2) \tag{4.2d}$$

B. Conservation of Mass in Each Element

Mass flux is solved using a finite volume approach similar to the one followed for small deformations. Here for each element, we obtain

$$\dot{C}_{0,e} = 0 \tag{4.3}$$

$$\dot{C}_{1,e} = \frac{2}{h^2} f_e \tag{4.4}$$

C. Helmholtz Free Energy and The Rate of Dissipation

Using the discretization mentioned above in equation 2.6, the Helmholtz free energy for a beam element is given by

$$\begin{aligned}\psi_e = \int_{ele} \frac{EI}{2}\frac{d^2N_j}{dx^2}\frac{d^2N_i}{dx^2}d_j d_i + EIkC_{1,e}\frac{d^2N_i}{dx^2}d_i \\ + \left(\frac{B+Ek^2}{2}\right)IC_{1,e}^2 + DIC_{1,e}q_e + \frac{q_e^2}{2p} + 2bh\left(\frac{B+Ek^2}{2}\right)C_{0,e}^2\end{aligned} \tag{4.5}$$

where '$\int_{ele}$' denotes integration over the length the element and repeated indices denote summation of that term over all possible index values.

We explicitly use the constraint (4.4) while defining the dissipation function for each element. The rate of dissipation in each element is given by

$$\xi_e = (Q\dot{C}_{1,e}^2 + R\dot{q}_e^2 + 2S\dot{C}_{1,e}\dot{q}_e)\Delta L \tag{4.6}$$

D. Governing Equations

Using the principle of maximum rate of dissipation hypothesis, we get the mechanical equilibrium equations for each beam element in the form $K^e_{ij}d_j = f^e_i$ where the matrix K^e_{ij} and the vector f^e_i are given by

$$K^e_{ij} = \frac{EI}{\Delta L^3}\begin{bmatrix} 12 & 6\Delta L & -12 & 6\Delta L \\ 6\Delta L & 4\Delta L^2 & -6\Delta L & 2\Delta L^2 \\ -12 & -6\Delta L & 12 & -6\Delta L \\ 6\Delta L & 2\Delta L^2 & -6\Delta L & 4\Delta L^2 \end{bmatrix} \tag{4.7}$$

$$f^e_i = P^e_i - EIkC_{1,e}(t)\begin{Bmatrix} 0 \\ -1 \\ 0 \\ 1 \end{Bmatrix} + \int_{ele} w(x)N_i(x) \tag{4.8}$$

In each element, $C_{1,e}$ varies according to

$$z\dot{C}_{1,e} = \left(\frac{S}{p} - DIR\right)q_e - \left(REIk^2 + RBI - DIS\right)C_{1,e} - V_eS - SEIk\frac{d_4 - d_2}{\Delta L} \tag{4.9}$$

where $z = (QR - S^2)$.

q_e varies according to

$$z\dot{q}_e = \left(SBI + SEIk^2 - QDI\right)C_{1,e} - \left(\frac{Q}{p} - DIS\right)q_e + QV_e + SEIk\frac{d_4 - d_2}{\Delta L} \tag{4.10}$$

To solve the coupled problem, we use a staggared time stepping algorithm similar to the one used for the large deformation problem. The details of the algorithm used for the numerical scheme presented here are shown in Algorithm 2. $\boldsymbol{d}$, $\boldsymbol{C_1}$ and $\boldsymbol{q}$ denote vectors of all discretized displacements, concentration slope, and charge respectively. Superscripts denotes discretization with respect to the time step.

Algorithm 2 Implementation of the Iterative Time-Stepping Scheme

1: Input: Initial conditions: displacement $\boldsymbol{d}^{(0)}$, ${\boldsymbol{C_1}}^{(0)}$ and $\boldsymbol{q}^{(0)}$,
time step of integration Δt, Model parameters, Tolerance TOL.
2: Set $\boldsymbol{d}^{(n)} = \boldsymbol{d}^{(0)}$, ${\boldsymbol{C_1}}^{(n)} = {\boldsymbol{C_1}}^{(0)}$, $q^{(n)} = q^{(0)}$
3: **while** Until Convergence, $\Delta \boldsymbol{d} \leq$ TOL **do**
4: Find ${\boldsymbol{C_1}}^{(n+1)}$ and $\boldsymbol{q}^{(n+1)}$ using $\boldsymbol{d}^{(n)}$
5: Find $\boldsymbol{d}^{(n)}$ using ${\boldsymbol{C_1}}^{(n+1)}$ and $\boldsymbol{q}^{(n+1)}$
6: $\Delta \boldsymbol{d} = \boldsymbol{d}^{(n+1)} - \boldsymbol{d}^{(n)}$
7: Set $\boldsymbol{d}^{(n)} = \boldsymbol{d}^{(n+1)}$, ${\boldsymbol{C_1}}^{(n)} = {\boldsymbol{C_1}}^{(0)}$, $\boldsymbol{q}^{(n)} = \boldsymbol{q}^{(0)}$
8: **end while**

In the next chapter we study the performance of the model using some test cases.

CHAPTER V

RESULTS

We analyze the performance of the model by comparing the simulation results with reported experimental data ([3]). Moreover we analyze the qualitative behaviour of the model and compare the responses of Flemion and Nafion based IPMC strips under some of the designers questions.

A. Parameters Used for Simulation

The parameters used in this simulation are given below.

1. TBA^+/Flemion IPMC Strip Parameters

$Nele = 10,\ TOL = 10^{-8},\ dt = 1\text{s},\ L = 32\text{mm},\ b = 3.4\text{mm},\ 2h = 0.17\text{mm},$
$E = 72\text{Mpa},\ k = 900(\text{no units}),\ I = 1.11\text{x}10^{-14}\text{m}^{-4},\ B = 5\text{x}10^{12}\text{Nm}^{-2},$
$D = 10^{12}\text{Nm}^{-2}\text{C}^{-1}, R = 340\text{ohm},\ p = 76\text{x}10^{-3}\text{F},\ Q = 7\text{Nm}^2\text{s},$
$S = 0.42\text{N}m^2\text{sC}^{-1}$

2. Li^+/Nafion IPMC Strip Parameters

$Nele = 10,\ TOL = 1e-8,\ dt = 0.01\text{s},\ L = 30\text{mm},\ b = 3\text{mm},\ 2h = 1\text{mm},$
$E = 72\text{Mpa},\ k = 900(\text{no units}),\ I = 2\text{x}10^{-12}\text{m}^{-4},\ B = 2\text{x}10^{13}\text{Nm}^{-2},$
$D = 6.2\text{x}10^{11}\text{Nm}^{-2}\text{C}^{-1}, R = 160\text{ohm},\ p = 80\text{x}10^{-3}\text{F},\ Q = 20\text{Nm}^2\text{s},$
$S = 45\text{Nm}^2\text{sC}^{-1}$

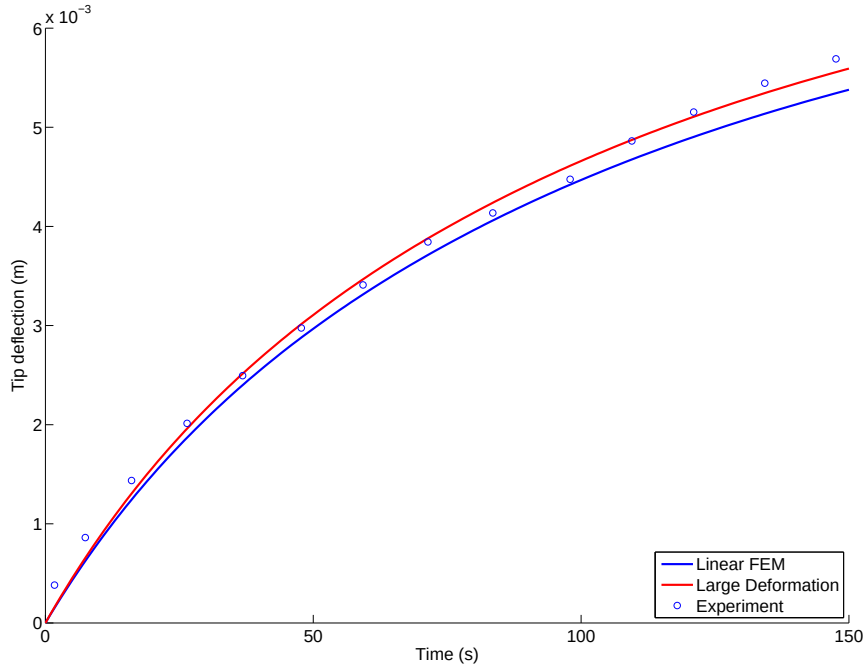

Fig. 9. Variation of Tip deflection with Time on application of a step voltage TBA^+/Flemion IPMC strip compared with experimental data from [3].

B. Comparison with Experimental Data

Tip deflection response of the TBA^+/Flemion IPMC strip under the application of a unit step voltage is shown in Figure 9. We see that the FEM solution under predicts the tip displacement in this case.

Tip displacement response of the Li^+/Nafion IPMC strip under the application of a unit step voltage is shown in Figure 10. We see that the FEM solution under predicts the tip displacement in this case.

Tip displacement response of the TBA^+/Flemion IPMC strip under the application of a unit step voltage and different end forces are shown in Figure 11. There is an initial elastic jump in the direction of the applied force followed by bending towards steady state values.

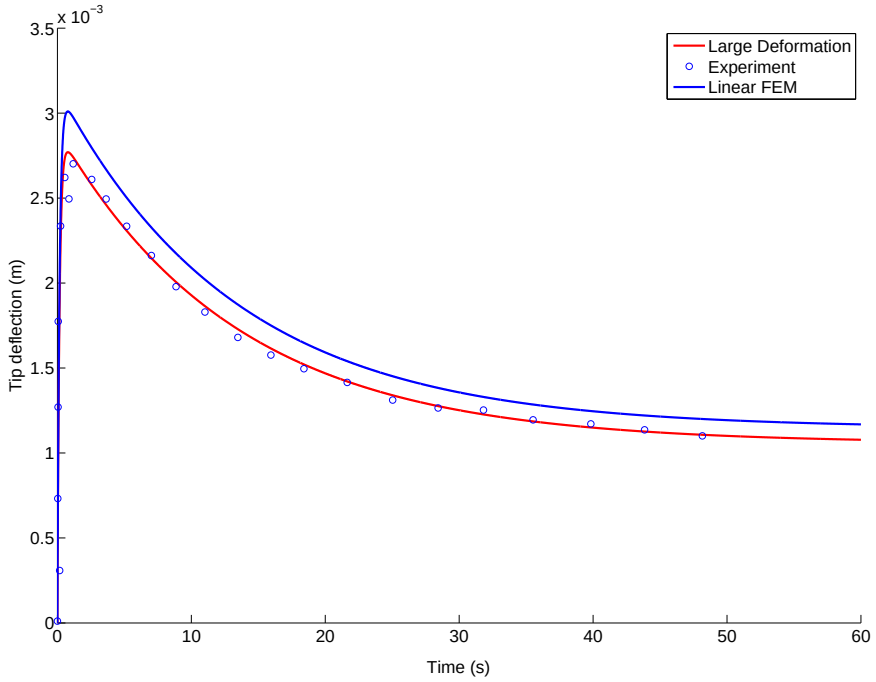

Fig. 10. Variation of Tip deflection with Time on application of a step voltage for a Li^+/Nafion IPMC strip compared with experimental data from [3].

Figure 12 shows the response of IPMC strips with different values for the nondimensional parameter S which determines the amount of convective heating. It is noticed that the convective heating term in the rate of dissipation function differs for IPMC strips with different polymer bases and is crucial for simulating different electromechanical responses exhibited by them.

C. Simulation of The Large Deformation Problem

We analyze some of the problems the large deformation formulation could handle. We also test the transient response of the Nafion and Flemion IPMC strips under the application of a sinusoidal voltage. Figure 13 shows a simulation of the Large Deformation Model for TBA^+/Flemion IPMC strip on application of a step voltage

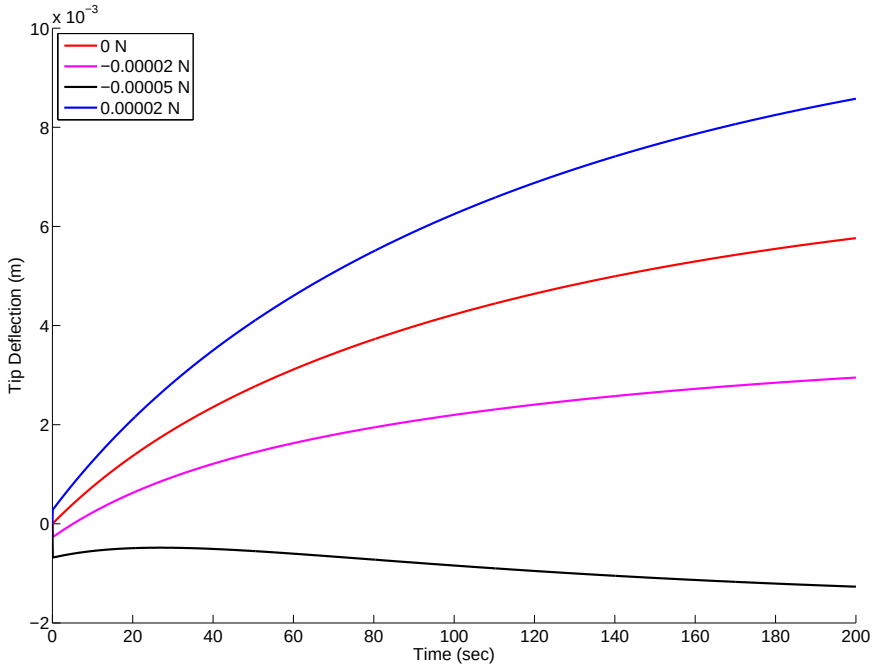

Fig. 11. Variation of Tip deflection with Time on application of a step voltage and different end forces for a TBA^+/Flemion IPMC strip.

of $5V$.

The finite difference scheme of the large deformation model is able to handle the loading case where the sign of the applied voltage is varied at the second half of the beam as shown in Figure 14.

D. Simulation of the Transient Response Under Sinusoidal Voltage

Figure 15 Response of Flemion strips lags behind that of the applied voltage. This has been reported experimentally. The Nafion strips seems to have a negative lag but it is due to the initial overshoot. This lag decreases as the frequency of the applied sinusoidal voltage decreases. Given the lag between the input voltage and the output displacement is lesser for Nafion based IPMC strips compared to that of Flemion

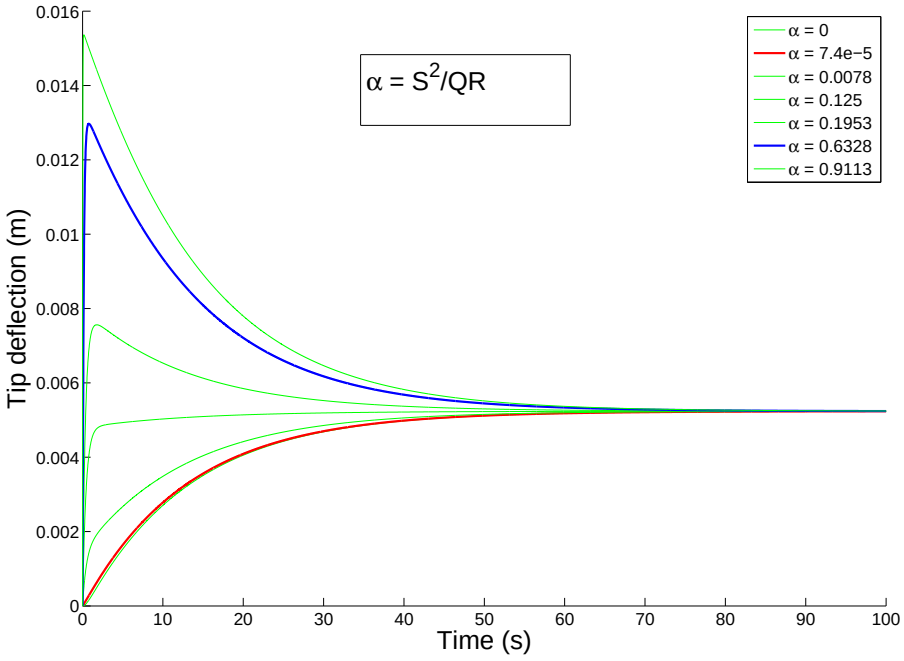

Fig. 12. Variation of Tip deflection with Time on application of a step voltage for different non-dimensionalized versions of the convective heating constant in the rate of dissipation. The red curve is for TBA^+/Flemion IPMC strips and the blue curve is for Li^+/Nafion IPMC strips.

based IPMC strips, the former would be better suited for control applications.

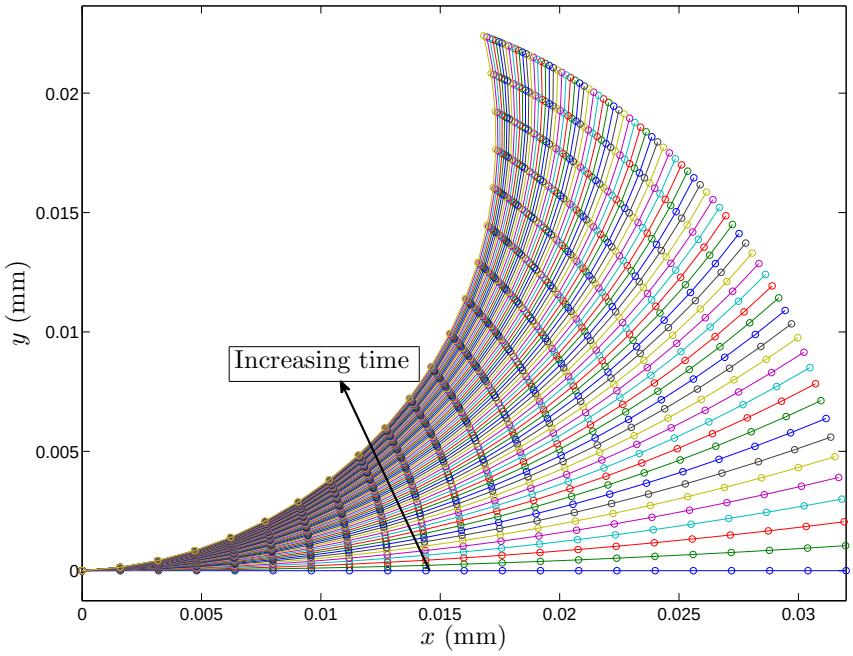

Fig. 13. Simulation of Large Deformation Model for TBA^+/Flemion IPMC strip on application of a step voltage of $5V$.

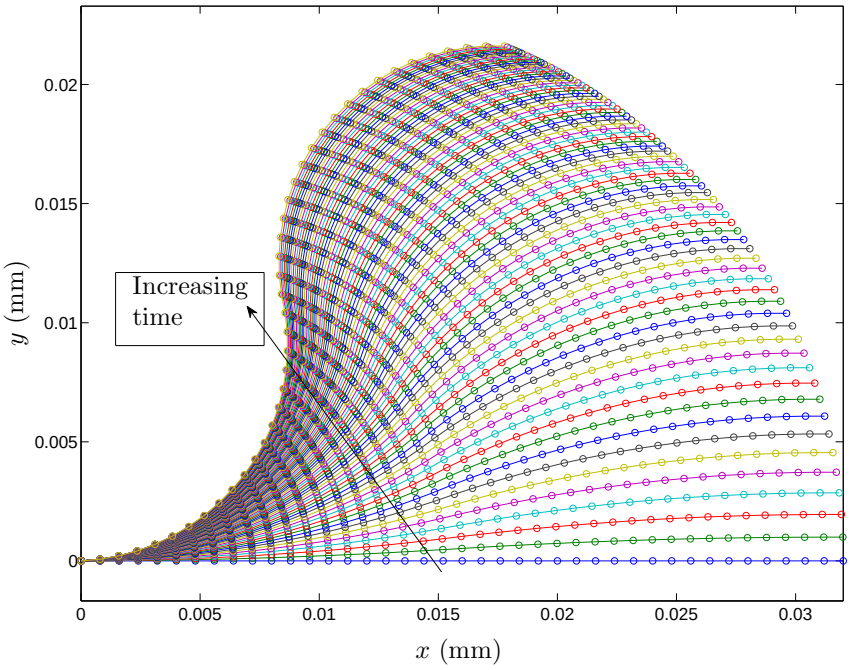

Fig. 14. Simulation of Large Deformation Model for TBA^+/Flemion IPMC strip on application of a step voltage of $10V$ to the first half of the beam and -$10V$ to the seconde half of the beam.

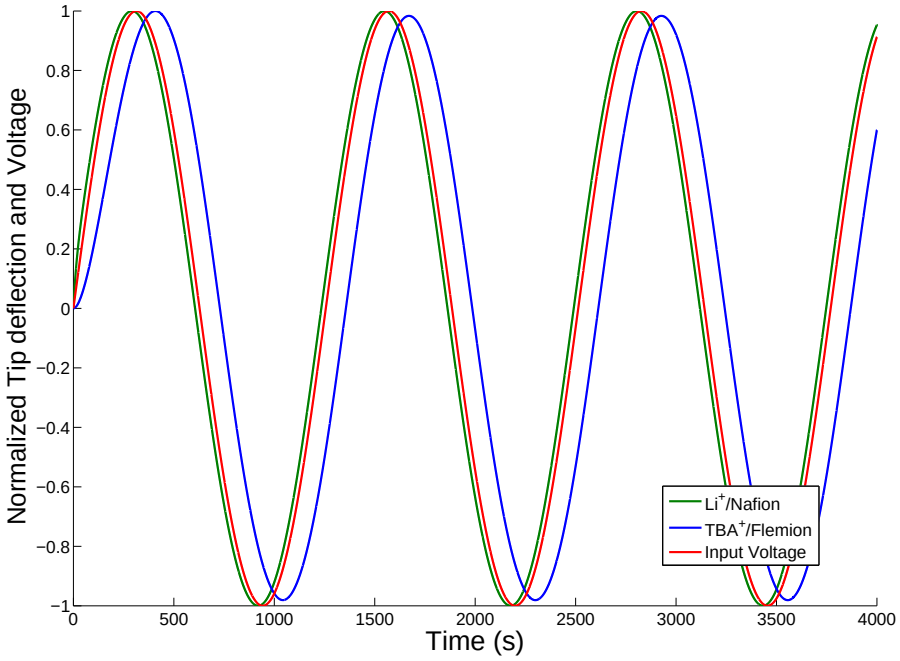

Fig. 15. Simulation of Large Deformation Model for TBA^+/Flemion and Li^+/Nafion IPMC strips on application of a sinusoidal input voltage of $1V$. The tip displacements are normalized with respect to the maximum value.

CHAPTER VI

CONCLUSION

A. Summary of Work Done

We developed a thermodynamically consistent model for IPMC strips based on Euler-Bernoulli beam theory. We formulated a linear finite element solution for the model and proposed a time stepping scheme to solve the coupled transient problem. Further, we extended the model to solve large deformations involving pure beding and proposed a finite difference solution. We showed that the model is able to simulate the electromechanical reponse of IPMC strips. The large deformation model was able to handle certain complicated electromechanical loading. We observed that Nafion based strips would be better suited for control applications. We also showed that the convective heating term in the rate of dissipation function is crucial for simulating different electromechanical responses exhibited by IPMC strips made of different polymer bases.

B. Further Work

- A method to determine the parameters of the model from experimental data.
- Finite element solution using Von Karman strain measure for problems involving large deformations.
- Characterize mateirial parameters for different compositions and combinations of counterions and polymer matrix.
- Actuation in water by considering flux in and out of the IPMC strips surface.

REFERENCES

[1] M. Shahinpoor and K.J. Kim, "Ionic polymer-metal composites: I. Fundamentals," *Smart Materials and Structures*, vol. 10, no. 4, pp. 819–833, 2001.

[2] Y. Bar-Cohen, X. Bao, S. Sherrit, and S.S. Lih, "Characterization of the electromechanical properties of ionomeric polymer-metal composite (IPMC)," 2002, `http://hdl.handle.net/2014/11866`.

[3] X. Bao, Y. Bar-Cohen, and S.S. Lih, "Measurements and macro models of ionomeric polymer-metal composites (IMPC)," *Proc. SPIE*, vol. 4695, pp. 220–227, 2002.

[4] M. Shahinpoor and K.J. Kim, "Ionic polymer–metal composites: IV. Industrial and medical applications," *Smart Materials and Structures*, vol. 14, no. 1, pp. 197–214, 2005.

[5] Y. Bar-Cohen, S. Leary, A. Yavrouian, K. Oguro, S. Tadokoro, J. Harrison, J. Smith, and J. Su, "Challenges to the transition of IPMC artificial muscle actuators to practical application," in *MRS Symposium Proceedings*, 1999, MS Document ID:31295.

[6] A. Menciassi and P. Dario, "Bio-inspired solutions for locomotion in the gastrointestinal tract: background and perspectives," *Philosophical Transactions of the Royal Society of London. Series A: Mathematical, Physical and Engineering Sciences*, vol. 361, no. 1811, pp. 2287–2298, 2003.

[7] Y. Bar-Cohen, "Electroactive polymers as artificial muscles-capabilities, potentials and challenges," in *Handbook on Biomimetics, Section 11, in Chapter 8*. Tokya, Japan: NTS Inc., 2000.

[8] Y. Bar-Cohen, *Electroactive Polymer (EAP) Actuators as Artificial Muscles: Reality, Potential, and Challenges*, Bellingham, WA: SPIE Press, 2004.

[9] S. Nemat-Nasser and Y. Wu, "Comparative experimental study of ionic polymer–metal composites with different backbone ionomers and in various cation forms," *Journal of Applied Physics*, vol. 93, no. 9, pp. 5255–5267, 2003.

[10] S. Nemat-Nasser, S. Zamani, and Y. Tor, "Effect of solvents on the chemical and physical properties of ionic polymer-metal composites," *Journal of Applied Physics*, vol. 99, pp. 104902, 2006.

[11] R. Tiwari and E. Garcia, "The state of understanding of ionic polymer metal composite architecture: a review," *Smart Materials and Structures*, vol. 20, pp. 083001, 2011.

[12] K.J. Kim and M. Shahinpoor, "Ionic polymer–metal composites: II. Manufacturing techniques," *Smart Materials and Structures*, vol. 12, no. 1, pp. 65–79, 2003.

[13] M. Shahinpoor and K.J. Kim, "Ionic polymer–metal composites: III. Modeling and simulation as biomimetic sensors, actuators, transducers, and artificial muscles," *Smart Materials and Structures*, vol. 13, no. 6, pp. 1362–1388, 2004.

[14] S. Nemat-Nasser and J.Y. Li, "Electromechanical response of ionic polymer-metal composites," *Journal of Applied Physics*, vol. 87, pp. 3321–3331, 2000.

[15] S. Nemat-Nasser and Y. Wu, "Tailoring the actuation of ionic polymer–metal composites," *Smart Materials and Structures*, vol. 15, no. 4, pp. 909–923, 2006.

[16] S. Tadokoro, S. Yamagami, T. Takamori, and K. Oguro, "An actuator model of ICPF for robotic applications on the basis of physicochemical hypotheses," in

Proceedings of IEEE Conference on Robotics and Automation, (ICRA), 2000, vol. 2, pp. 1340–1346.

[17] PJ Costa Branco and JA Dente, "Derivation of a continuum model and its electric equivalent-circuit representation for ionic polymer–metal composite (IPMC) electromechanics," *Smart Materials and Structures*, vol. 15, no. 2, pp. 378–392, 2006.

[18] T. Wallmersperger, A. Horstmann, B. Kroplin, and D.J. Leo, "Thermodynamical modeling of the electromechanical behavior of ionic polymer metal composites," *Journal of Intelligent Material Systems and Structures*, vol. 20, no. 6, pp. 741–750, 2009.

[19] P. Nardinocchi, M. Pezzulla, and L. Placidi, "Thermodynamically based multiphysic modeling of ionic polymer metal composites," *Journal of Intelligent Material Systems and Structures*, vol. 22, no. 16, pp. 1887–1897, 2011.

[20] M. Porfiri, "An electromechanical model for sensing and actuation of ionic polymer metal composites," *Smart Materials and Structures*, vol. 18, no. 1, pp. 015016 (11), 2009.

[21] G.D. Bufalo, L. Placidi, and M. Porfiri, "A mixture theory framework for modeling the mechanical actuation of ionic polymer metal composites," *Smart Materials and Structures*, vol. 17, no. 4, pp. 045010 (14), 2008.

[22] S. Nemat-Nasser, "Micromechanics of actuation of ionic polymer-metal composites," *Journal of Applied Physics*, vol. 92, no. 5, pp. 2899–2915, 2002.

[23] P.G. Gennes, K. Okumura, M. Shahinpoor, and KJ Kim, "Mechanoelectric effects in ionic gels," *Europhysics Letters*, vol. 50, no. 4, pp. 513–518, 2000.

[24] K. Bhattacharya, J. Li, and Y. Xiao, *Electromechanical Models for Optimal Design and Effective Behavior of Electroactive Polymers*, Bellingham, WA: SPIE Press, 2001.

[25] K. Farinholt and D.J. Leo, "Modeling of electromechanical charge sensing in ionic polymer transducers," *Mechanics of Materials*, vol. 36, no. 5, pp. 421–433, 2004.

[26] Z. Chen, X. Tan, A. Will, and C. Ziel, "A dynamic model for ionic polymer–metal composite sensors," *Smart Materials and Structures*, vol. 16, no. 4, pp. 1477–1488, 2007.

[27] K.M. Newbury and D.J. Leo, "Electromechanical modeling and characterization of ionic polymer benders," *Journal of Intelligent Material Systems and Structures*, vol. 13, no. 1, pp. 51–60, 2002.

[28] T. Osada, K. Takagi, Y. Hayakawa, Z.W. Luo, and K. Asaka, "State space modeling of ionic polymer-metal composite actuators based on electrostress diffusion coupling theory," in *Proceedings of IEEE/RSJ International Conference on Intelligent Robots and Systems, (IROS)*, 2008, pp. 119–124.

[29] K.M. Newbury and D.J. Leo, "Linear electromechanical model of ionic polymer transducers-part I: Model development," *Journal of Intelligent Material Systems and Structures*, vol. 14, no. 6, pp. 333–342, 2003.

[30] J.W. Paquette, K.J. Kim, J.D. Nam, and Y.S. Tak, "An equivalent circuit model for ionic polymer-metal composites and their performance improvement by a clay-based polymer nano-composite technique," *Journal of Intelligent Material Systems and Structures*, vol. 14, no. 10, pp. 633–642, 2003.

[31] SP Girrens and FW Smith, "Constituent diffusion in a deformable thermoelastic solid," *Journal of Applied Mechanics*, vol. 54, no. 2, pp. 441–446, 1987.

[32] S. Baek and AR Srinivasa, "Diffusion of a fluid through an elastic solid undergoing large deformation," *International Journal of Non-linear Mechanics*, vol. 39, no. 2, pp. 201–218, 2004.

[33] A.R. Srinivasa and S.M. Sivakumar, *Inelasticity of Materials: An Engineering Approach and a Practical Guide*, Hackensack, NJ: World Scientific, 2009.

APPENDIX A

MRDH FOR SMALL DEFORMATIONS

The external loads considered here are a distributed load $w(x)$ and an applied electric potential $V(x)$. From the Power theorem,

$$\int_0^L (wv_o + V\dot{q})\ dx = \int_0^L (\dot{\psi} + \xi)\ dx \tag{A.1}$$

$$\dot{\psi} = \frac{\partial \psi}{\partial v_o''}\dot{v}_o'' + \frac{\partial \psi}{\partial C_1}\dot{C}_1 + \frac{\partial \psi}{\partial q}\dot{q} \tag{A.2a}$$

$$\frac{\partial \psi}{\partial v_o''} = EIv_o'' + EIkC_1 \tag{A.2b}$$

$$\frac{\partial \psi}{\partial C_1} = (B + Ek^2)IC_1 + EIkv_o'' + DIq \tag{A.2c}$$

$$\frac{\partial \psi}{\partial q} = DIC_1 + \frac{q}{p} \tag{A.2d}$$

Using the method of Lagrange multipliers, the rate of dissipation is maximized considering the mass conservation equation (2.10) and the Power theorem (equation (A.1)) as constraints. Considering a new function Φ with Lagrange multipliers λ and μ,

$$\Phi = \int_0^L \xi + \lambda \left(- \int_0^L (wv_o + V\dot{q})\ dx + \int_0^L (\dot{\psi} + \xi)\ dx \right) + \mu \dot{C}_0 \tag{A.3}$$

$$\begin{aligned} \frac{\partial \Phi}{\partial \dot{v}_0} = 0 = \int_0^L & \left(EI(v_0'''' + kC_1'') - w\right)\ dx \\ & + \left(EI(v_0'' + kC_1) - M\right)\dot{v}_0'\big|_{x=0} + \left(EI(v_0'' + kC_1) - M\right)\dot{v}_0'\big|_{x=L} \\ & + \left(EI(v_0''' + kC_1') - F\right)\dot{v}_0\big|_{x=0} + \left(EI(v_0''' + kC_1') - F\right)\dot{v}_0\big|_{x=L} \end{aligned} \tag{A.4}$$

which gives the mechanical equilibrium equation (2.14) along with the boundary conditions (2.15).

$$\frac{\partial \Phi}{\partial \dot{C}_0} = 0 = \mu \tag{A.5}$$

$$\frac{\partial \Phi}{\partial \dot{C}_1} = 0 = 2(1+\lambda)\int_0^L (Q\dot{C}_1 + S\dot{q})\ dx - \lambda \int_0^L \frac{\partial \psi}{\partial C_1}\ dx \tag{A.6}$$

$$\frac{\partial \Phi}{\partial \dot{q}} = 0 = 2(1+\lambda)\int_0^L (S\dot{C}_1 + R\dot{q})\ dx - \lambda \int_0^L \left(\frac{\partial \psi}{\partial q} - V\right)\ dx \tag{A.7}$$

Minimizing with respect to λ and μ we get the constraint equations (A.1) and (2.10) respectively.

Using equations (A.6), (A.7), (A.4) and (A.1),

$$\begin{aligned}\frac{\partial \Phi}{\partial \dot{q}}\dot{q} + \frac{\partial \Phi}{\partial \dot{C}_1}\dot{C}_1 &= 0 \\ &= 2(1+\lambda)\int_0^L \xi\ dx - \lambda \int_0^L \left(\frac{\partial \psi}{\partial C_1}\dot{C}_1 + \frac{\partial \psi}{\partial q}\dot{q} - V\dot{q}\right)\ dx \\ &= 2(1+\lambda)\int_0^L \xi\ dx - \lambda \int_0^L \xi\ dx\end{aligned} \tag{A.8}$$

which gives $2(1+\lambda) = \lambda$ or $\lambda = -2$. Using this in equations (A.7) and (A.6), we get equations (2.16) and (2.17) that govern the transient response.

APPENDIX B

MRDH FOR LARGE DEFORMATIONS INVOLVING PURE BENDING

From the Power theorem

$$M\dot{\theta}(L) + \int_0^L V\dot{q}\ ds = \int_0^L (\dot{\psi} + \xi)\ ds \tag{B.1}$$

$$\dot{\psi} = \frac{\partial \psi}{\partial \theta}\dot{\theta} + \frac{\partial \psi}{\partial C_1}\dot{C}_1 + \frac{\partial \psi}{\partial q}\dot{q} \tag{B.2a}$$

$$\frac{\partial \psi}{\partial \theta} = EI\frac{d\theta}{ds} + EIkC_1 \tag{B.2b}$$

$$\frac{\partial \psi}{\partial C_1} = (B + Ek^2)IC_1 + EIk\frac{d\theta}{ds} + DIq \tag{B.2c}$$

$$\frac{\partial \psi}{\partial q} = DIC_1 + \frac{q}{p} \tag{B.2d}$$

Using the method of Lagrange multipliers, the rate of dissipation is maximized with the mass conservation equation $\dot{C}_0 = 0$ and the Power theorem (equation (B.1)) as constraints. Considering a new function Φ with Lagrange multipliers λ and μ,

$$\Phi = \int_0^L \xi + \lambda\left(-M\dot{\theta}(L) + \int_0^L (-V\dot{q} + \dot{\psi} + \xi)\ ds\right) + \mu\dot{C}_0 \tag{B.3}$$

$$\begin{aligned}\frac{\partial \Phi}{\partial \dot{\theta}} = 0 = \int_0^L \left(\frac{d^2\theta}{ds^2} + k\frac{dC_1}{ds}\right)\ ds \\ + \left(EI\frac{d\theta(s)}{ds} + EIkC_1(s) - M\right)\dot{\theta}\Big|_{s=0} \\ + \left(EI\frac{d\theta(s)}{ds} + EIkC_1(s) - M\right)\dot{\theta}\Big|_{s=L}\end{aligned} \tag{B.4}$$

which gives the mechanical equilibrium equation (3.4) along with the boundary conditions (3.5).

$$\frac{\partial \Phi}{\partial \dot{C}_0} = 0 = \mu \tag{B.5}$$

$$\frac{\partial \Phi}{\partial \dot{C}_1} = 0 = 2(1+\lambda)\int_0^L (Q\dot{C}_1 + S\dot{q})\ ds - \lambda \int_0^L \frac{\partial \psi}{\partial C_1}\ ds \tag{B.6}$$

$$\frac{\partial \Phi}{\partial \dot{q}} = 0 = 2(1+\lambda)\int_0^L (S\dot{C}_1 + R\dot{q})\ ds - \lambda \int_0^L \left(\frac{\partial \psi}{\partial q} - V\right)\ ds \tag{B.7}$$

Minimizing with respect to λ and μ we get the constraint equations (B.1) and (**??**) respectively.

Using equations (B.6), (B.7), (B.4) and (B.1),

$$\begin{aligned}\frac{\partial \Phi}{\partial \dot{q}}\dot{q} + \frac{\partial \Phi}{\partial \dot{C}_1}\dot{C}_1 &= 0 \\ &= 2(1+\lambda)\int_0^L \xi\ ds - \lambda \int_0^L \left(\frac{\partial \psi}{\partial C_1}\dot{C}_1 + \frac{\partial \psi}{\partial q}\dot{q} - V\dot{q}\right)\ ds \\ &= 2(1+\lambda)\int_0^L \xi\ ds - \lambda \int_0^L \xi\ ds\end{aligned} \tag{B.8}$$

which gives $2(1+\lambda) = \lambda$ or $\lambda = -2$. Using this in equations (B.7) and (B.6), we get equations (3.6) and (3.7) that govern the transient response.

APPENDIX C

MRDH FOR FEM

The external loads considered here are a distributed load $w(x)$, generalized loads P_i and an applied electric potential at the element V_e. The work done by the external forces is

$$W = P_i^e \dot{d}_i + V_e \dot{q}_e \Delta L + \int_{ele} w(x) \dot{v}_0 dx \tag{C.1a}$$

$$= P_i^e \dot{d}_i + V_e \dot{q}_e \Delta L + \int_{ele} w(x) N_i \dot{d}_i dx \tag{C.1b}$$

From the Power theorem

$$P_i^e \dot{d}_i + V_e \dot{q}_e \Delta L + \int_{ele} w(x) N_i \dot{d}_i \; dx = \xi_e + \int_{ele} \dot{\psi}_e \; dx \tag{C.2}$$

$$\dot{\psi} = \frac{\partial \psi}{\partial d_i} \dot{d}_i + \frac{\partial \psi}{\partial C_1} \dot{C}_1 + \frac{\partial \psi}{\partial q} \dot{q} \tag{C.3a}$$

$$\frac{\partial \psi}{\partial d_i} = EI \frac{d^2 N_j}{dx^2} \frac{d^2 N_i}{dx^2} d_j + EIkC_{1,e} \frac{d^2 N_i}{dx^2} \tag{C.3b}$$

$$\frac{\partial \psi}{\partial C_{1,e}} = (B + Ek^2) IC_{1,e} + EIk \frac{d^2 N_i}{dx^2} d_i + DIq_e \tag{C.3c}$$

$$\frac{\partial \psi}{\partial q_e} = DIC_{1,e} + \frac{q_e}{p} \tag{C.3d}$$

Using the method of Lagrange multipliers, the rate of dissipation is maximized considering the mass conservation equation (4.4) and the Power theorem (equation (C.2)) as constraints. Considering a new function Φ with Lagrange multipliers λ and μ

$$\Phi = \int_{ele} \xi + \lambda \left(-P_i^e \dot{d}_i - V_e \dot{q}_e \Delta L - \int_{ele} (w N_i \dot{d}_i) \; dx + \xi_e + \int_{ele} \dot{\psi}_e \; dx \right) + \mu \dot{C}_{0,e} \tag{C.4}$$

$$\frac{\partial \Phi}{\partial \dot{d}_i} = 0 = \int_{ele} \left(EI \frac{d^2 N_j}{dx^2} \frac{d^2 N_i}{dx^2} d_j + EIkC_{1,e} \frac{d^2 N_i}{dx^2} - wN_i \right) \, dx - P_i^e \tag{C.5}$$

which gives the mechanical equilibrium equationin the form $K_{ij}^e d_j = f_i^e$ for each element.

$$\frac{\partial \Phi}{\partial \dot{C}_{0,e}} = 0 = \mu \tag{C.6}$$

$$\frac{\partial \Phi}{\partial \dot{C}_{1,e}} = 0 = 2(1+\lambda)(Q\dot{C}_{1,e} + S\dot{q})\Delta L - \lambda \int_{ele} \frac{\partial \psi}{\partial C_{1,e}} \tag{C.7}$$

$$\frac{\partial \Phi}{\partial \dot{q}_e} = 0 = 2(1+\lambda)(S\dot{C}_{1,e} + R\dot{q}_e)\Delta L - \lambda V_e \Delta L - \lambda \frac{\partial \psi}{\partial q_e} \Delta L \tag{C.8}$$

Minimizing with respect to λ and μ we get the constraint equations (C.2) and (4.4) respectively.

Using equations (C.7), (C.8), (C.5) and (C.2),

$$\begin{aligned} \frac{\partial \Phi}{\partial \dot{q}_e} \dot{q}_e + \frac{\partial \Phi}{\partial \dot{C}_{1,e}} \dot{C}_{1,e} &= 0 \\ &= 2(1+\lambda)\xi_e - \lambda V_e \dot{q}_e \Delta L - \lambda \frac{\partial \psi}{\partial q_e} \dot{q}_e \Delta L - \lambda \int_{ele} \frac{\partial \psi}{\partial C_{1,e}} \dot{C}_{1,e} \\ &= 2(1+\lambda)\xi_e - \lambda \xi_e \end{aligned} \tag{C.9}$$

which gives $2(1+\lambda) = \lambda$ or $\lambda = -2$. Using this in equations (C.8) and (C.7), we get equations (4.10) and (4.10) that govern the transient response for each element.

VITA

Jayavel Arumugam received a Bachelor of Technology degree in civil engineering from the Indian Institute of Technology - Madras in 2009. After finishing his Master of Science degree in mechanical engineering, he is continuing for a Ph.D. degree in mechanical engineering at Texas A&M University. His research interests include thermodynamical modelling and numerical solutions of diffusion-deformation coupled problems. Address: 411 James J. Cain '51 Building (ENPH), Texas A&M University, College Station, TX 77843–3368.